Purdue University Purdue e-Pubs

Birck and NCN Publications

Birck Nanotechnology Center

8-5-2008

Electrowetting-based control of droplet transition and morphology on artificially microstructured surfaces

Vaibhav Bahadur

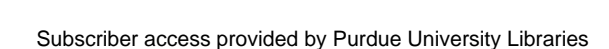
Purdue University - Main Campus, vbahadur@purdue.edu

Suresh Garimella
School of Mechanical Engineering, sureshg@purdue.edu

Follow this and additional works at: http://docs.lib.purdue.edu/nanopub

Bahadur, Vaibhav and Garimella, Suresh, "Electrowetting-based control of droplet transition and morphology on artificially microstructured surfaces" (2008). *Birck and NCN Publications*. Paper 141. http://docs.lib.purdue.edu/nanopub/141

This document has been made available through Purdue e-Pubs, a service of the Purdue University Libraries. Please contact epubs@purdue.edu for additional information.





Research Article

Electrowetting-Based Control of Droplet Transition and Morphology on Artificially Microstructured Surfaces

Vaibhav Bahadur, and Suresh V. Garimella

Langmuir, 2008, 24 (15), 8338-8345 • DOI: 10.1021/la800556c • Publication Date (Web): 04 July 2008

Downloaded from http://pubs.acs.org on November 19, 2008



More About This Article

Additional resources and features associated with this article are available within the HTML version:

- Supporting Information
- · Access to high resolution figures
- Links to articles and content related to this article
- Copyright permission to reproduce figures and/or text from this article

View the Full Text HTML



Electrowetting-Based Control of Droplet Transition and Morphology on Artificially Microstructured Surfaces

Vaibhav Bahadur and Suresh V. Garimella*

School of Mechanical Engineering and Birck Nanotechnology Center, Purdue University, West Lafayette, Indiana 47907-2088

Received February 20, 2008. Revised Manuscript Received April 23, 2008

Electrowetting (EW) has recently been demonstrated as a powerful tool for controlling droplet morphology on smooth and artificially structured surfaces. The present work involves a systematic experimental investigation of the influence of electrowetting in determining and altering the state of a static droplet resting on an artificially microstructured surface. Extensive experimentation is carried out to benchmark a previously developed energy-minimization-based model that analyzed the influence of interfacial energies, surface roughness parameters, and electric fields in determining the apparent contact angle of a droplet in the Cassie and Wenzel states under the influence of an EW voltage. The EW voltage required to trigger a transition from the Cassie state to the Wenzel state is experimentally determined for surfaces having a wide range of surface parameters (surface roughness and fraction of surface area covered with pillars). The reversibility of the Cassie—Wenzel transition upon the removal of the EW voltage is also quantified and analyzed. The experimental results from the present work form the basis for the design of surfaces that enable dynamic control of droplet morphology. A significant finding from the present work is that nonconservative dissipative forces have a significant influence in opposing fluid flow inside the microstructured surface that inhibits reversibility of the Cassie—Wenzel transition. The artificially structured surfaces considered in this work have microscale roughness feature sizes that permits direct visual observation of EW-induced Cassie—Wenzel droplet transition; this is the first reported visual confirmation of EW-induced droplet state transition.

1. Introduction

Electrowetting (EW) involves the electrical control of solid—liquid interfacial tension¹ and has many applications involving microscale flow control in areas such as laboratory-on-chip systems, biomedical devices, and other MEMS-based fluidic devices. The traditional concept of EWOD (electrowetting on dielectric) is founded on the premise of an effective reduction in the dielectric—liquid interfacial energy by the application of a voltage between a conducting droplet and an underlying dielectric layer. EW has been used to demonstrate droplet actuation^{2–10} and other microfluidic operations, such as the formation, mixing, and splitting of droplets.¹¹ There has also been significant progress in understanding the governing phenomena that influence EW systems, such as the EW-induced

actuation force, ¹² contact angle saturation, ¹³ the role of the electric double layer, ¹⁴ and dynamics of the three-phase line. ¹⁵

The contact angle of a droplet shows a strong dependence on the morphology of the surface on which it rests. The influence of surface roughness on the apparent contact angle of the droplet is generally understood by a study of two theoretically extreme situations as described in detail by Bahadur and Garimella. ¹⁶ In the Cassie state ¹⁷ (Figure 1a) the droplet base rests on the tips of the roughness elements; consequently, the droplet is in composite contact with air and solid at its base. In the Wenzel state ¹⁸ (Figure 1b) the droplet fills the grooves between the roughness elements and is in intimate contact with the solid surface. Surface roughness can significantly alter the contact angle of a droplet and change its effective contact area with the surface. Since EW also acts to change the droplet contact angle, surface design can be used in conjunction with EW for enhanced control of droplet contact angles.

The influence of surface roughness on liquid wettability has been studied ^{19,20} with the objective of developing superhydrophobic surfaces for use in laboratory-on-chip applications. He et al. ²¹ provided experimental evidence showing that both Cassie and Wenzel droplet formation is possible on the same surface depending on the way the droplets are formed. Patankar ¹⁹ showed that the surface energy of the Cassie and Wenzel droplets is minimized when the apparent (macroscopic) contact angle equals

 $^{*\} Corresponding\ author.\ E-mail:\ sureshg@purdue.edu.$

⁽¹⁾ Kim, C. J. ASME International Mechanical Engineering Congress and Exposition, New York, 2001; IMECE2001/HTD-24200.

⁽²⁾ Pollack, M. G.; Shenderov, A. D.; Fair, R. B. Lab Chip 2002, 2, 96.

⁽³⁾ Mohseni, K.; Dolatabadi, A. 43rd AIAA Aerospace Science Meeting and Exhibit, Reno, NV, 2005; AIAA-677.

⁽⁴⁾ Kuo, J. S.; Spicar-Mihalic, P.; Rodriguez, I.; Chiu, D. T. *Langmuir* **2003**, *19*, 250.

⁽⁵⁾ Yi, U. C.; Kim, C. J. 13th International Conference on Solid-State Sensors, Actuators and Microsystems, Seoul, South Korea, 2005.

⁽⁶⁾ Torkkeli, A.; Saarilahti, J.; Haara, A.; Harma, H.; Soukka, T.; Tolonen, P. 14th International IEEE Conference on MEMS, 2001; 475–478.

⁽⁷⁾ Oprins, H.; Vandevelde, B.; Beyne, E.; Borghs, G.; Baelmans, M. International Workshop on Thermal Investigations of ICs and Systems, Cote d'Azur, France, 2001; 207–212.

⁽⁸⁾ Chatterjee, D.; Hetayothin, B.; Wheeler, A. R.; King, D. J.; Garrell, R. L. Lab Chip 2006, 6, 199.

⁽⁹⁾ Paik, P.; Pamula, V. K.; Chakrabarty, K. Proceedings of IMECE 2005, Orlando, FL, 2005; IMECE2005–81081.

⁽¹⁰⁾ Cooney, C. G.; Chen, C.; Emerling, M. R.; Sterling, J. D. *Microfluidics Nanofluidics* 2006.

⁽¹¹⁾ Fair, R. B.; Srinivasan, V.; Ren, H.; Paik, P.; Pamula, V. K.; Pollack, M. G. IEEE International Electron Devices Meeting, 2003.

⁽¹²⁾ Bahadur, V.; Garimella, S. V. J. Micromech. Microeng. 2006, 16, 1494.

⁽¹³⁾ Quilliet, C.; Berge, B. Curr. Opin. Colloid Interface Sci. 2001, 2, 34.
(14) Quinn, A.; Sedev, R.; Ralston, J. J. Phys. Chem. B 2003, 107, 1163.

⁽¹⁵⁾ Blake, T. D. Surfactant Science Series 49; Marcel Dekker: New York, 1993; pp 251-309.

⁽¹⁶⁾ Bahadur, V.; Garimella, S. V. Langmuir 2007, 23, 4918.

⁽¹⁷⁾ Cassie, A. B. D. Discuss. Faraday Soc. 1948, 3, 11.

⁽¹⁸⁾ Wenzel, T. N. J. Phys. Colloid Chem. 1949, 3, 1466.

⁽¹⁹⁾ Patankar, N. A. Langmuir 2003, 19, 1249.

⁽²⁰⁾ Kim, J.; Kim, C. J. IEEE Conference MEMS, Las Vegas, NV, 2002; 479-482.

⁽²¹⁾ He, B.; Patankar, N. A.; LeeJ., Langmuir 2003, 19, 4999.

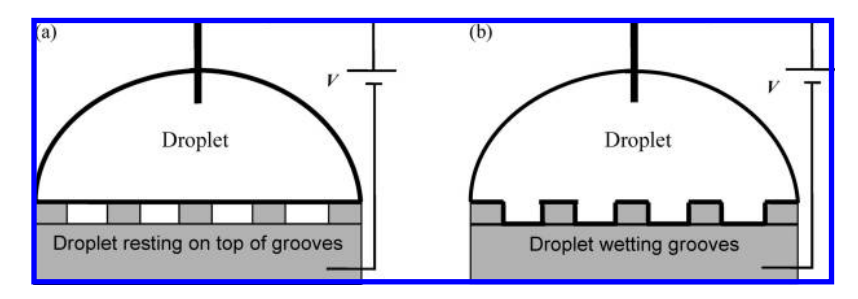


Figure 1. Droplet states on electrowetted rough surfaces: (a) Cassie state and (b) Wenzel state.

that predicted by the Cassie and Wenzel equations. However, the Cassie and Wenzel droplets differ in their surface energies, and the stable equilibrium state of the droplet corresponds to the state that has a lower energy. Patankar²² also analyzed the transition of a droplet from the Cassie state to the lower energy Wenzel state on artificially roughened surfaces (without an EW voltage) and discussed the presence of an energy barrier for the Cassie-Wenzel transition.

The influence of EW on droplet behavior on rough surfaces has been the focus of a few recent research efforts. Krupenkin et al.²³ demonstrated that a droplet resting on a nanostructured surface can be made to transition to a completely wetting (Wenzel) state from an initial superhydrophobic (Cassie) state by the application of an EW voltage. Herbertson et al.24 investigated EW on rough surfaces by measuring the contact angle of a droplet on a patterned SU-8 photoresist surface under the influence of an EW voltage. The SU-8 surface in this work provided the necessary roughness in addition to its role as the dielectric layer. Zhu et al.²⁵ characterized the behavior of water droplets on vertically aligned carbon nanotube surfaces under the influence of an electrowetting voltage and experimentally investigated the limits of contact angle change on such surfaces. Wang et al.²⁶ studied the effect of an EW voltage on the contact angle of a static water droplet resting on a vertically aligned multiwalled carbon nanotube film covered with a conformal Parylene layer. Wang et al.²⁷ demonstrated the abrupt transition of a water droplet from a superhydrophobic (Cassie) state to a hydrophilic (Wenzel) state on an aligned multiwalled carbon nanotube array upon the application of an EW voltage. Bahadur and Garimella 16 developed an energy-minimization-based modeling approach to estimate the contact angle of a droplet in the Cassie and Wenzel states under the influence of an EW voltage and to predict the droplet transition under the influence of an EW voltage. The models developed were selectively benchmarked by application to the experimental results of Krupenkin et al.²³ and Herbertson et al.²⁴ The models from ref 16 are further benchmarked and analyzed in the present work to ascertain their applicability to the design of artificially structured surfaces for enabling dynamic control of droplet morphology.

A key characteristic in the study of EW on artificially structured surfaces concerns the reversibility of the EW-induced Cassie-Wenzel transition. Krupenkin et al.23 and Herbertson et al.24 did not observe a reverse transition to the Cassie state upon removal of the EW voltage. Krupenkin et al.²⁸ recently demonstrated the reverse transition upon passing a heat pulse through the substrate while the droplet was in the Wenzel state, thereby evaporating a part of the liquid adjacent to the substrate. Dhindsa et al.²⁹ studied the reversibility of EW transition of a saline droplet resting on a vertically aligned carbon nanofiber film. A saline droplet in an air environment did not exhibit any reversibility; however, EW experiments on a saline droplet immersed in a dodecane oil bath showed complete reversibility upon the removal of the EW voltage. Contact angle visualization and system capacitance measurements were used to confirm the Cassie-Wenzel transition. Verplanck et al.³⁰ recently demonstrated reversibility of the EW-induced Cassie-Wenzel transition of a saline droplet resting on a superhydrophobic silicon nanowire surface in ambient air. Contact angle measurements were provided to demonstrate the reversibility of the EW transition; however, the physics enabling the reverse transition was not discussed. The existence of an energy barrier has been proposed by various researchers^{22,28,31} as the primary reason for the irreversibility of the Cassie-Wenzel transition even when the Cassie state is of lower energy than the Wenzel state.

The primary objective of the present work is to experimentally characterize the EW-induced droplet transition on artificially microstructured silicon surfaces in an air environment and use the experimental results to assess the models developed by Bahadur and Garimella. 16 The structured surfaces examined in the present work feature roughness elements of microscale dimensions, a roughness regime that is much larger than the nanoscale dimensions typically used to design superhydrophobic surfaces. ^{23,26,29,30} The use of such microscale roughness features permits a direct visual observation of EW-induced transition. Previous approaches have relied upon indirect methods such as contact angle visualization, measurement of contact-angle hysteresis, capacitance measurements, and the use of photodefinable droplets²³ to study the occurrence of transition. The approach in the present work presents a direct method of observing the transition, enabling a more detailed study of droplet transition. A second objective of the present work is the study of the reversibility of the Cassie-Wenzel transition on such microstructured surfaces. Two distinct and independent criteria are proposed to measure and quantify the extent of the reversibility of the Cassie-Wenzel transition. It is shown that dissipative forces that comprise contact-line friction, contact-line pinning, and shear resistance to fluid motion inside the microstructured surface exert a strong influence (along with the energy barrier to the reverse transition) in preventing complete reversibility of

⁽²²⁾ Patankar, N. A. Langmuir 2004, 20, 7097.

⁽²³⁾ Krupenkin, T. N.; Taylor, J. A.; Schneider, T. M.; Yang, S. Langmuir **2004**, 20, 3824.

⁽²⁴⁾ Herbertson, D. J.; Evans, R. E.; Shirtcliffe, N. J.; McHale, G.; Newton, M. I. Sensors Actuators A 2006, 130, 189.

⁽²⁵⁾ Zhu, L.; Xu, J.; Xiu, Y.; Sun, Y.; Hess, D. W.; Wong, C. J. Phys. Chem. B 2006, 110, 15945.

⁽²⁶⁾ Wang, Z.; Ou, Y.; Lu, T.; Koratkar, N. J. Phys. Chem. B 2007, 111, 4296. (27) Wang, Z.; Ci, L.; Chen, L.; Nayak, S.; Ajayan, P.; Koratkar, N. Nano Lett. **2007**, 7, 697.

⁽²⁸⁾ Krupenkin, T. N.; Taylor, J. A.; Wang, E. N.; Kolodner, P.; Hodes, M.; Salamon, T. R. Langmuir 2007, 23, 9128.

⁽²⁹⁾ Dhindsa, M.; Smith, N. R.; Heikenfeld, J.; Rack, P. D.; Fowlkes, J. D.; Doktycz, M. J.; Melechko, A. V.; Simpson, M. L. Langmuir 2006, 22, 9030. (30) Verplanck, N.; Galopin, E.; Camart, J.; Thomy, V.; Coffinier, Y.; Boukherrouub, *Nano Lett.* **2007**, *7*, 813.

⁽³¹⁾ Nosonovsky, M.; Bhushan, B. Langmuir 2008, 24, 1525.

the Cassie—Wenzel transition upon removal of the EW voltage. Partial reversibility is seen on certain microstructured surfaces, whereby the droplet remains in the Wenzel state but retracts to a higher contact angle upon the removal of the EW voltage.

2. Artifically Microstructured Surfaces: Design and Fabrication

In the Cassie state, the droplet sits on a composite surface of air and solid (Figure 1a). The apparent contact angle θ_C of such a droplet can be obtained 32 from the energy-minimization principle as

$$\cos \theta_C = -1 + \varphi (1 + \cos \theta_0) \tag{1}$$

where φ is the ratio of the area of the top surface of the pillars to the total base area of the substrate and θ_0 is the contact angle of the droplet on a flat surface. The hydrophobicity of a Cassie droplet increases as φ decreases because of enhanced contact with air. In the Wenzel state, the droplet is in intimate contact with the surface features. For such a droplet, the apparent contact angle θ_W is similarly obtained 32 as

$$\cos \theta_{\rm W} = r_{\rm m} \cos \theta_0 \tag{2}$$

where $r_{\rm m}$ is the surface roughness defined as the ratio of the total surface area (including the sides and base) of the roughness elements to the projected surface area (not including the sides) of the roughness elements). The Wenzel state thus amplifies the initial hydrophobicity or hydrophilicity of the droplet. Equation 2 predicts that the cosine of the apparent contact angle will increase linearly with surface roughness. However, eq 2 is not valid for high surface roughness values, as discussed by Quere, ³² since the absolute value of the cosine is always less than 1.

Bahadur and Garimella¹⁶ developed expressions for the apparent contact angle of a droplet resting on a structured surface in the presence of an EW voltage. The surface considered was electrically conducting and was coated with a thin dielectric layer of thickness d and dielectric constant k that conformed to the surface roughness features. An EW field was established across the dielectric by electrodes contacting the conducting droplet and the electrically conducting substrate. The dimensions of the droplet were such that the effect of gravity was neglected; consequently, the droplet assumed the shape of a truncated sphere. An energy-minimization framework was used to estimate the contact angle $\theta_{\rm E}^{\rm E}$ of a droplet in the Cassie state under the influence of an EW voltage V as 16

$$\cos \theta_{\rm C}^{\rm E} = -1 + \varphi (1 + \cos \theta_0 + \eta) \tag{3}$$

where η is the electrowetting number expressed as

$$\eta = \frac{k\varepsilon_0 V^2}{2d\gamma_{\rm LA}^0} \tag{4}$$

A similar procedure was applied to estimate the apparent contact angle θ_W^E of a Wenzel drop under the influence of an EW voltage as 16

$$\cos \theta_{\rm W}^{\rm E} = r_{\rm m}(\cos \theta_0 + \eta) \tag{5}$$

Patankar¹⁹ showed that the surface energy of a constant-volume droplet can be expressed solely in terms of the apparent contact angle. Furthermore, the droplet surface energy increases with the apparent contact angle of the droplet. This implies that the lower of the Cassie and Wenzel angles corresponds to the stable equilibrium position of the droplet. EW can be employed to

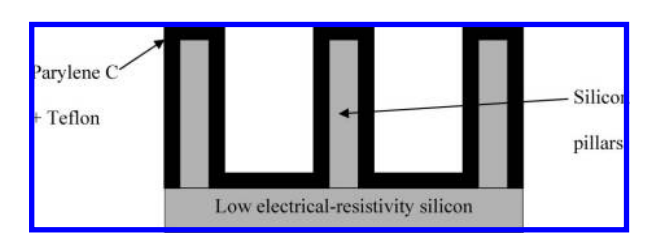


Figure 2. Schematic illustration of the silicon-based microstructured surface used in the experiments.

design surfaces on which the droplet states are manipulated dynamically by changing the relative energy content (and relative stability) of the Cassie and Wenzel states. The surfaces need to be designed such that the Cassie state is more favorable energetically than the Wenzel state in the absence of an EW voltage that is satisfied by the following relation ¹⁶ between the surface roughness parameters $r_{\rm m}$ and φ :

$$\cos \theta_0 < -\frac{(1-\varphi)}{(r_{\rm m} - \varphi)} \tag{6}$$

Application of an EW voltage can lower the energy of the electrowetted Wenzel state in comparison to the electrowetted Cassie state and thereby trigger a transition to the Wenzel state. Bahadur and Garimella¹⁶ estimated the minimum EW number required for a transition to the Wenzel state as

$$\eta > -\cos\theta_0 - \frac{(1-\varphi)}{(r_{\rm m} - \varphi)} \tag{7}$$

Droplet transition at a voltage predicted by the above equation requires additional activation energy for the droplet to successfully overcome the energy barrier to transition as described by Bahadur and Garimella. ¹⁶ This requirement of activation energy can be eliminated if the EW number η is further increased such that

$$\eta > -\cos \theta_0$$
 (8)

Equations 1–8 form the basis for the design of the microstructured surfaces in the present work. A cross section of the silicon microstructured surfaces fabricated for the present work is shown schematically in Figure 2. The microstructured surfaces consist of patterned silicon pillars covered with a thin layer of Parylene C (which acts as the EW dielectric) and a thin layer of Teflon (for hydrophobicity). The minimum feature size of all the roughness elements was fixed to be greater than 10 $\mu \rm m$ to enable direct visual observation of the EW-induced droplet state transition. The roughness-causing elements were selected to be square pillars, arranged with a uniform square pitch. For a surface morphology described by square pillars of width a and pitch b and with pillar height h, the roughness parameters $r_{\rm m}$ and φ can be expressed as

$$r_{\rm m} = 1 + \frac{4ah}{h^2} \tag{9}$$

and

$$\varphi = \frac{a^2}{b^2} \tag{10}$$

Twelve surfaces of varying surface parameters were fabricated and characterized in the present work. Table 1 shows the surface parameters $r_{\rm m}$ and φ and the pillar height h of the 12 surfaces that were designed for experimentation with water droplets. These surfaces are classified into three groups based on the range of φ values. In the rest of this paper, the surfaces with nominal φ

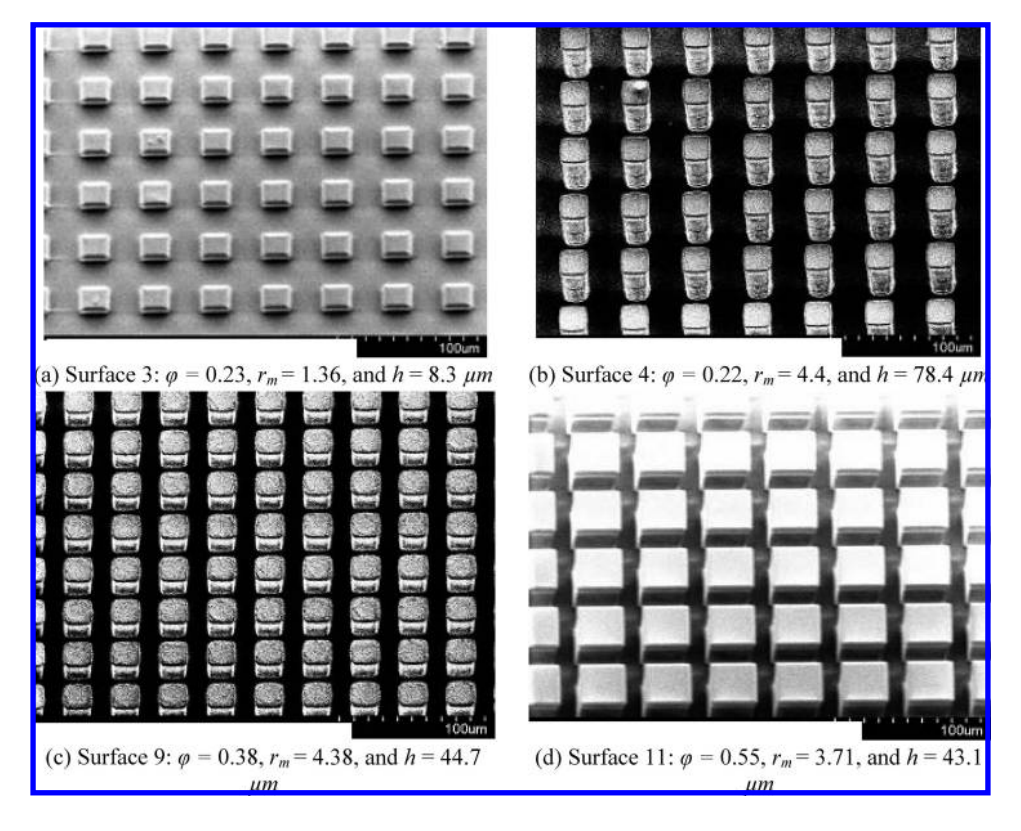


Figure 3. Scanning electron microscopy (SEM) images of four representative microstructured surfaces fabricated in the present work: surface 3, $\varphi = 0.23$, $r_{\rm m} = 1.36$, and $h = 8.3 \,\mu{\rm m}$; (b) surface 4, $\varphi = 0.22$, $r_{\rm m} = 4.4$, and $h = 78.4 \,\mu{\rm m}$; (c) surface 9, $\varphi = 0.38$, $r_{\rm m} = 4.38$, and $h = 44.7 \,\mu{\rm m}$; and (d) surface 11, $\varphi = 0.55$, $r_{\rm m} = 3.71$, and $h = 43.1 \ \mu {\rm m}$.

values of 0.2, 0.4, and 0.55 are referred to as low, medium, and high φ -value surfaces, respectively.

All the microstructured surfaces in the present work were fabricated at the Birck Nanotechnology Center of Purdue University. All the chemicals and etchants utilized during the fabrication process were clean-room grade. Highly doped (low electrical resistivity) silicon ((100) orientation) wafers covered with a layer of 1 μ m thermally grown oxide were used as the substrate. The low electrical resistivity ensured the requisite electrical conductivity for the application of an EW voltage. Positive photoresist was photolithographically patterned to selectively mask the underlying oxide layer by creating features representing the roughness causing pillars. Silicon dioxide was then selectively etched away by employing a wet etch process. The patterned oxide layer served as the mask for a subsequent deep reactive ion etch (DRIE) process using SF₆ and C₄F₈, which was employed to fabricate the silicon pillars. The silicon pillars were then conformally coated with a Parylene C layer by a physical vapor deposition process. Three different Parylene C thicknesses $(0.81, 1.2, \text{ and } 1.45 \,\mu\text{m})$ were selected in order to study the effect of the Parylene Clayer thickness on the EW-induced Cassie-Wenzel transition voltage. Finally, 1% by weight of Teflon AF1600 (DuPont, Wilmington, DE) in a solution of FC 77 (3M, St. Paul, MN) was spun on the structured surface to impart superhydrophobicity. Both the Parylene C and Teflon deposition processes led to conformal coatings as verified from scanning electron microscope (SEM) images. Figure 3a-d shows SEM images of four representative microstructured surfaces. The microstructured surfaces presented in Figure 3 span almost the entire range of the φ values (0.22–0.55), the entire range of $r_{\rm m}$ values (1.36–4.4), and the entire range of pillar heights $(8.3-78.4 \mu m)$.

3. Experimental Results: EW-Induced Control of **Droplet States on Microstructured Surfaces**

This section describes the results of experiments carried out to study EW-induced control of static droplet states on microstructured surfaces. An important feature of the experiments consists of direct visual observation of the EW-induced transition. Figure 4 shows

Table 1. Specifications of the Microstructured Surfaces Designed for the Electrowetting Experiments

						contact angle without EW (deg)	
surface number	φ	$r_{ m m}$	pillar height h (μ m)	dielectric layer thickness (μm)	stable state without EW	predicted	observed
1	0.18	1.37	8.3	0.81	Wenzel	125	128
2	0.21	2.74	36.5	1.45	Cassie	151	150
3	0.23	1.36	8.3	0.81	Wenzel	125	130
4	0.22	4.4	78.4	1.2	Cassie	151	152
5	0.23	2.87	43.1	0.81	Cassie	150	157
6	0.41	1.63	8.3	0.81	Wenzel	134	148
7	0.41	1.91	12.1	0.81	Cassie	140	148
8	0.41	2.83	24.2	0.81	Cassie	140	149
9	0.38	4.38	44.7	1.2	Cassie	141	154
10	0.55	1.52	8.3	0.81	Wenzel	130	138
11	0.55	3.71	43.1	0.81	Cassie	133	145
12	0.59	2.5	23.0	1.45	Cassie	131	138

Figure 4. Droplet states on electrowetted rough surfaces. The droplet on the left is in the Cassie state in the absence of an EW voltage, but transitions to the Wenzel state (shown on the right) at an EW voltage of 80 V.

a water droplet resting on a microstructured surface with $r_{\rm m}$ = 3, $\varphi = 0.43$ and a pillar height of 31 μ m. The droplet on the left is clearly in the Cassie state in the absence of an EW voltage as is evident from the background light visible between the pillars. This image was obtained by carefully aligning the surface with the light source and adjusting the aperture of the camera to admit the maximum amount of light. This direct visual confirmation of the existence of the Cassie state is similar to the experiments of He et al.²¹ and Jung et al.,³³ in which the visibility of light between the pillars was used to verify the existence of the Cassie state. The white circular region near the center of the droplet images is an optical effect caused from the backlighting. The droplet was observed to transition to the Wenzel state (shown on the right in Figure 4) upon the application of an EW voltage of 80 V. The EW voltage was applied using a wire penetrating the droplet as seen on the top of the droplet in Figure 4. The existence of the Wenzel state is also directly confirmed, since no background light is visible through the pillars, which are filled with water. This method of direct observation of droplet states was utilized in all the experiments in this work to determine the onset of transition. For surfaces with low pillar heights or high φ values, direct observation was not very conclusive, because high pillar significantly density sed the available area for light passage in the Cassie state. Therefore, the onset of transition was also verified by mechanically dragging the droplet. A droplet in the Cassie state offers significantly lesser resistance to motion than a droplet in the Wenzel state. This obvious difference in drag resistance was utilized in conjunction with droplet imaging to identify the onset of transition. It is important to note that the pillars fabricated in the present work were communicating in nature; consequently, the air is expelled through the spaces between the pillars when the droplet transitions to the Wenzel state.

The sixth column in Table 1 shows the observed state of wetting of a deionized water droplet on each of the 12 surfaces in the absence of an EW voltage. Equation 6 predicts the stable state of a droplet (in the absence of an EW voltage), which depends on the surface parameters $r_{\rm m}$ and φ . The predictions agree with the experimentally observed droplet states (shown in Table 1) for all the 12 surfaces. Eight of the 12 surfaces in the present work were designed such that the Cassie state was more stable than the Wenzel state in the absence of an EW voltage; these surfaces were utilized to study the EW-induced Cassie—Wenzel transition. The remaining four surfaces were designed such that the Wenzel state was the more stable state (in the absence of an EW voltage); these surfaces were utilized to study the role of dissipative forces during EW-induced droplet spreading in the

Wenzel state. The last two columns of Table 1 show the predicted (using eqs 1 and 2) and observed contact angles of water droplets on the structured surfaces in the absence of an EW voltage. The observed contact angles in Table 1 were measured using the image processing software accompanying the goniometer. Table 1 shows that the observed and predicted contact angles agree reasonably well (to within 10%) for all of the surfaces tested in the present work. The volume of the droplets in all the experiments was less than 5 μ L; for this range of droplet sizes, gravity is insignificant as compared to surface forces.

3a. Measurement of EW Voltages for the Cassie-Wenzel Transition. The first set of experiments determined the EW voltage needed to trigger a transition from the Cassie state to the Wenzel state. Bahadur and Garimella 16 showed that the minimum EW voltage necessary to trigger a transition to the Wenzel state is given by eq 7 and depends on the roughness parameters $r_{\rm m}$ and φ . However, additional activation energy is needed at this value of the EW voltage to successfully overcome the energy barrier to transition. This requirement of an activation energy can be eliminated if the EW voltage is increased to the limit predicted by eq 8, i.e., $(\eta > -\cos \theta_0)$. It is significant that this EW voltage (predicted by eq 8) does not depend on the surface roughness parameters $r_{\rm m}$ or φ ; in other words, it is expected to be the same for all the surfaces examined in the present work. This important prediction from the model was directly verified in the present work. No attempt was made to benchmark eq 7, however, since the origin and nature of the energy barrier to transition is still not clearly understood.

The transition voltage predicted by eq 8 depends on the dielectric layer properties (thickness and dielectric constant) and the droplet fluid surface tension. The only experimental parameter that was varied in the present work was the thickness of the Parylene C dielectric layer. Consequently, the surfaces with the largest (1.45 μ m) and smallest (0.81 μ m) thicknesses of Parylene were selected for experimentation to benchmark eq 8; the five surfaces with these dielectric layer thicknesses are extracted in Table 2. A deionized water droplet was gently deposited on these surfaces and a 125 μ m-diameter chrome wire was inserted in the droplet to supply the EW voltage. The voltage was ramped up in steps of 5 V until the occurrence of complete transition was observed. Three experiments were conducted on each of the five surfaces and the average values of the experimentally observed transition voltages are presented in Table 2. Table 2 also shows the predicted value of the transition voltage (according to eq 8) at which the droplet will transition spontaneously to the Wenzel state without the requirement of an activation energy. It is seen that the experimentally observed transition voltages match the predicted values reasonably well, and the transition voltage (approximately 55 or 70 V, depending on dielectric thickness) is indeed seen to be independent of the surface roughness parameters $r_{\rm m}$ and φ . It is important to note that droplet-state transition can also be achieved at lower voltages (as predicted by eq 7), if additional activation energy is provided to the droplet to overcome the energy barrier. Partial transition was indeed observed in certain experiments at voltages lower than those predicted by eq 8. However, the nature and form of the activation energy required to overcome the energy barrier is not wellunderstood, and consequently, no attempt was made to study droplet transitions at voltages lower than those predicted by eq 8. An increase in dielectric layer thickness increases the EW voltage necessary to trigger a transition; this trend is clearly visible from the experimental results shown in Table 1. The magnitude of the experimentally observed transition voltages was greater than the predicted voltages for most of the

Table 2. EW Voltages Required To Effect Cassie-Wenzel Transition

surface number	φ	$r_{ m m}$	pillar height h (μ m)	dielectric layer thickness (μm)	transition voltage (V)	
					predicted	observed
5	0.23	2.87	43.1	0.81	43	35
8	0.41	2.83	24.2	0.81	43	55
11	0.55	3.71	43.1	0.81	43	58
12	0.59	2.5	23	1.45	57.6	73.3
2.	0.21	2.74	36.5	1.45	57.6	68.3

Table 3. Contact Angle Retraction on Microstructured Surfaces

surface number	φ	$r_{ m m}$	pillar height h (μ m)	% retraction
1	0.18	1.37	8.3	42.6
3	0.23	1.36	8.3	63.8
5	0.23	2.87	43.1	6.6
6	0.41	1.63	8.3	59.2
7	0.41	1.91	12.1	29.2
8	0.41	2.83	24.2	18.2
10	0.55	1.52	8.3	34.5
11	0.55	3.71	43.1	16.5

experiments. This can be attributed to frictional and dissipative forces that are not accounted for in the analytical model $^{\bar{1}6}$ and which increase the voltage beyond that predicted by eq 8.

3b. Reversibility of the Cassie-Wenzel Transition. The second set of experiments was carried out with the objective of studying the reversibility of the Cassie—Wenzel transition. Two distinct and independent criteria for the study of reversibility are introduced and studied in the present work. The first consists of the extent to which the contact angle retracts upon the removal of the EW voltage, while the second is an examination of whether the original Cassie state (for the surfaces in which the Cassie state is the starting state) is attained upon removal of the EW voltage. Both these criteria must be satisfied to conclude a complete reversibility of the transition. It is important to note that complete retraction of the contact angle upon removal of the EW voltage does not in itself indicate complete transition reversibility. To illustrate this point, the predicted Cassie and Wenzel angles for surface 7 ($r_{\rm m} = 1.91$ and $\varphi = 0.41$) are 140° and 144°, respectively; measurement of contact angle retraction is therefore an insufficient indicator of reversibility, since the contact angles are similar in value in the non-EW Cassie and Wenzel states. An examination of the retraction to the Cassie state is therefore essential in addition to contact angle retraction measurements to quantify the extent of transition reversibility. In the present work, the eight surfaces with a dielectric layer thickness of 0.81 μ m were selected for transition reversibility experiments and are listed in Table 3. The experiments consisted of applying an EW voltage of 100 V (sufficient to induce the Cassie—Wenzel transition) to the droplet and then reverting to 0 V. Droplet contact angles were measured before and after the application of the EW voltage and after the removal of the EW voltage. The extent of contact angle retraction was measured as a fraction of the contact angle change occurring upon the application of the EW voltage. The return to the Cassie state (five of the eight surfaces were designed to have the Cassie state as the stable state in the absence of an EW voltage) was measured by direct visual observation of the structured surfaces, as described earlier in this section.

The most significant observation from these experiments was that the retraction of the droplet to the Cassie state (upon the removal of the EW voltage) was not observed for any of the five surfaces that had the Cassie state as the more stable state in the absence of an EW voltage. This observation agrees with the observations of Krupenkin et al.,²³ who did not observe any reverse transition in their experiments. The contact angle retracted upon the removal of the EW voltage, and the extent of the

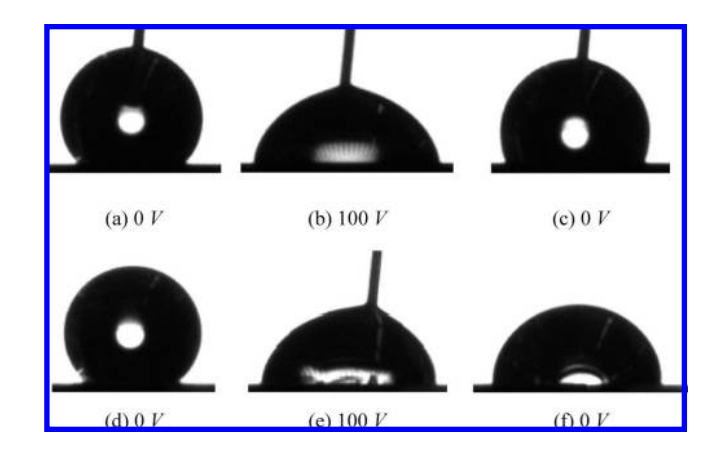


Figure 5. Contact angle retraction on microstructured surfaces: (a-c) a droplet on surface 3 with $r_{\rm m} = 1.36$ showing significant contact angle retraction and (d-f) a droplet on surface 11 with $r_{\rm m} = 3.71$ showing poor contact angle retraction. (a) 0 V, (b) 100 V, (c) 0 V, (d) 0 V, (e) 100 V, (f) 0 V.

retraction was seen to depend significantly on the surface roughness. Figure 5 shows droplet images on two different surfaces showing contrasting tendencies with respect to contact angle retraction. Figure 5a-c shows droplet images on surface 3, which has a roughness $r_{\rm m}$ of 1.36; for this surface, the droplet is in the Wenzel state even in the absence of an EW voltage. It can be seen that a high degree of contact angle retraction is observed on this surface upon the removal of the EW voltage. Figure 5d-f shows droplet images on surface 11, which has a roughness $r_{\rm m}$ of 3.71; for this surface, the droplet is in the Cassie state in the absence of an EW voltage. It can be seen that this surface shows little contact angle retraction upon the removal of the EW voltage.

Table 3 shows numerical values of the contact angle retraction for each of the eight surfaces considered in this study. The results show a clear dependence of the contact angle retraction on the surface roughness; higher roughness for the same value of φ leads to lesser retraction of the contact angles (as is evident from the results of experiments carried out on sets of surfaces 3-5, 6-8, and 10, 11). The contact angle retraction did not show a strong dependence on φ in the present experiments. Droplet reversibility experiments were also carried out on two other surfaces (4 and 9) with higher surface roughnesses than the surfaces in Table 3; for these two surfaces, the contact angle retraction upon the removal of EW voltage was essentially negligible. These results show that contact angle retraction on an artificially structured surface is very strongly influenced by the surface roughness.

There are two factors inhibiting complete reversibility of the droplet upon the removal of the EW voltage. The first is the energy barrier^{22,28,31} to transition to the Cassie state from the Wenzel state upon the removal of the EW voltage. Appropriate surface design can ensure that the Cassie state is more stable than the Wenzel state in the absence of an EW voltage; however, there still exists a barrier to transition from the Wenzel to the Cassie state, as described in detail for the present application by

Figure 6. Surface energy content of a droplet during transition ($r_m = 1.91$ and $\varphi = 0.41$). The bottom curve shows the surface energy variation during the EW-induced transition to the Wenzel state, and the top curve shows the surface energy variation during the reverse transition to the Cassie state with no EW.

Bahadur and Garimella. ¹⁶ This energy barrier can be more clearly understood with the aid of Figure 6, which shows the variation of droplet energy as it progressively wets the grooves. The amount of wetting can be expressed in terms of an effective roughness r with the condition $(1 \le r \le r_m)$; r = 1 corresponds to the Cassie state, whereas $r = r_{\rm m}$ corresponds to the Wenzel state. The total droplet surface energy is measured in terms of the droplet contact angle (an increase in the contact angle increases the droplet energy). The surface considered in Figure 6 is surface 7, which has a roughness $r_{\rm m}$ of 1.91 and a φ of 0.41. The lower curve in Figure 6 shows the energy content of the electrowetted Cassie state, the electrowetted Wenzel state, and the intermediate transition states as the droplet wets the grooves at an EW voltage represented by $\eta = 0.55$ (corresponding to 60 V). The contact angle at an intermediate transition state has been estimated by the energy-minimization principle¹⁶ to be

$$\theta_{\text{tr}}^{\text{E}} = \cos^{-1}((r-1+\varphi)(\cos\theta_0 + \eta) - 1 + \varphi)$$
 (11)

The downward slope of the lower curve in Figure 6 indicates a spontaneous transition of the droplet to a Wenzel state upon the application of the EW voltage. The upper curve in Figure 6 shows the energy of the droplet in the Cassie and Wenzel states as well as the energy content during the intermediate transition states for a reverse transition to the Cassie state (upon the removal of EW voltage). The application of an EW voltage triggers a spontaneous transition from the Cassie to the Wenzel state. Upon the removal of the EW voltage, the droplet needs a certain activation energy (as shown in Figure 6) to overcome the energy barrier to transition from the Wenzel state to the Cassie state. This requirement of activation energy is one of the factors that inhibits reversibility of the EW-induced state transition.

The second factor inhibiting droplet reversibility arises from various dissipative forces that oppose fluid motion. These dissipative forces are nonconservative in nature and have not been accounted for in the energy-minimization model of Bahadur and Garimella. The primary dissipative forces opposing EW-induced droplet motion on a *smooth* surface have been studied in detail by various researchers. Bahadur and Garimella showed contact-line friction and wall shear stress as the dominant dissipative forces for such systems. For the case of an EW-induced droplet transition to a Wenzel state, contact-line pinning

at the pillar edges also offers substantial resistance to fluid motion in addition to contact-line friction and viscous forces. The strength of all these dissipative forces increases with surface roughness; consequently, the contact angle retraction is impeded as the surface roughness increases, as shown in Table 3.

The experiments in the present section were also intended to highlight the importance of dissipative forces in influencing reversibility (in addition to the well-known energy barrier for the reverse transition). While the energy barrier for the reverse transition does not vary significantly for the surfaces considered in the present work, the role of dissipative forces in inhibiting reversibility can be clearly understood through these experiments on surfaces of varying roughness (with the dissipative forces depending on the roughness). Further, surfaces 1, 3, 6, and 10 (as shown in Table 3) were designed for a droplet to attain the Wenzel state even in the absence of an EW voltage; the absence of complete CA retraction on these surfaces can be attributed only to dissipative forces, since there is no possibility of an energy barrier for a reverse transition. These results underline the importance of considering dissipative forces along with energy barrier considerations while analyzing droplet transition reversibility.

Another set of experiments was carried out to quantify the strong influence of the dissipative forces, especially in the Wenzel regime. The experiments involved ramping up the EW voltage in steps of 20 V and measuring the droplet contact angle at each step (starting from the droplet in the Cassie state). Figure 7 shows the voltage-dependent contact angle of a deionized water droplet on surface 2, which has a $r_{\rm m}$ of 2.74 and φ of 0.21. It is seen from the figure that the experimental contact angles in the electrowetted Cassie state match the predicted contact angles (using eq 3) reasonably well. Predictions of contact angle (using eq 5) when the droplet transitions to the Wenzel state did not agree with the measured values and are not shown in Figure 7. The lack of agreement can be attributed to the dominance of dissipative forces in the Wenzel state, which have not been included in the model. On other surfaces in the present work the contact angle variation in the Wenzel state exhibited a stick-slip kind of behavior, which can be attributed to contact-line pinning at the walls of the roughness causing pillars. These experiments further reinforce the importance of dissipative forces in influencing

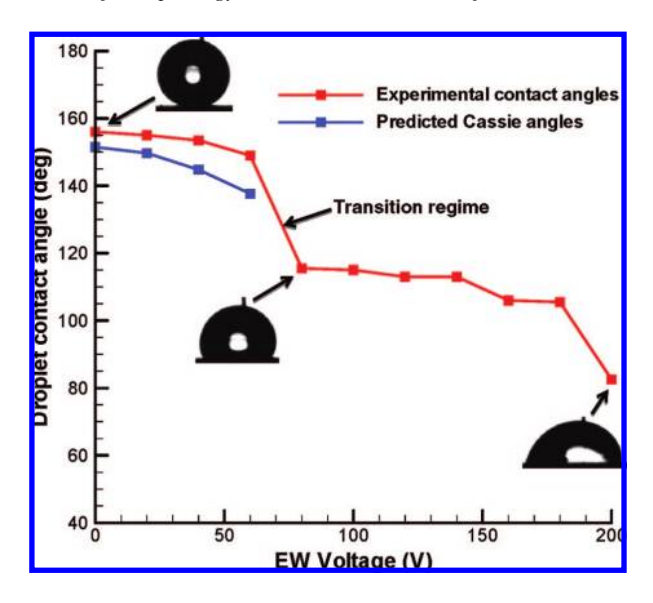


Figure 7. Droplet contact angle dependence on EW voltage ($r_{\rm m} = 2.74$ and $\varphi = 0.21$).

droplet morphology, especially in the Wenzel regime. To summarize, the present experiments indicate that the presence of an energy barrier and the dissipative forces are the two major factors inhibiting droplet state reversibility. The values of $r_{\rm m}$ and φ determine the energy barrier for the reverse transition, with the strength of the dissipative forces being primarily dependent

on $r_{\rm m}$. These opposing forces need to be further understood, quantified, and factored into the surface design to enable reversible surfaces for dynamic control of droplet morphology.

4. Conclusions

A careful and systematic experimental investigation of the influence of EW in determining and altering the state of a static droplet resting on artificially microstructured surfaces featuring a wide range of surface roughness $r_{\rm m}$ and φ values was presented in this work. Direct visual observation enabled the study of two specific aspects of droplet state transition: the EW voltage required for the Cassie—Wenzel transition and the reversibility of the transition upon the removal of the EW voltage. The EW voltages required for the Cassie—Wenzel transition showed reasonable agreement with the predicted values. It was seen that the existence of an energy barrier for the reverse transition and the roughness-dependent dissipative forces are the major factors that inhibit droplet reversibility.

The present results indicate that dissipative forces need to be minimized to enable the reverse transition. The nature and strength of these dissipative forces can be better understood by detailed modeling of the dynamics of wetting of the grooves. A study of the role of the shape and size of the roughness elements will also facilitate the design of surfaces that enable reversible transition. The results from the present work constitute a starting point for the design of surfaces in applications that require dynamic control of droplet morphology.

LA800556C